IOPscience iopscience.iop.org

Home Search Collections Journals About Contact us My IOPscience

Suppression of impurity and interface-roughness back-scattering in double quantum wires: theory beyond the Born approximation

This article has been downloaded from IOPscience. Please scroll down to see the full text article.

2000 J. Phys.: Condens. Matter 12 3383

(http://iopscience.iop.org/0953-8984/12/14/314)

View the table of contents for this issue, or go to the journal homepage for more

Download details:
IP Address: 171.66.16.221
The article was downloaded on 16/05/2010 at 04:46

Please note that terms and conditions apply.

J. Phys.: Condens. Matter **12** (2000) 3383–3396. Printed in the UK PII: S0953-8984(00)06847-8

Suppression of impurity and interface-roughness back-scattering in double quantum wires: theory beyond the Born approximation

Danhong Huang† and S K Lyo‡

† Air Force Research Laboratory (AFRL/VSSS), Kirtland Air Force Base, NM 87117, USA
‡ Sandia National Laboratories, Albuquerque, NM 87185, USA

Received 11 August 1999, in final form 28 February 2000

Abstract. The effect of higher-order corrections to the Born approximation is studied for the previously obtained giant conductance enhancement in tunnel-coupled double quantum wires in a magnetic field by including both impurity and interface-roughness scattering. The enhancement is caused by an abrupt suppression of back-scattering of electrons which occurs when the chemical potential is in the anticrossing gap of the ground tunnel-split doublet. The calculated conductance enhancement is large, and the relative higher-order correction to the enhancement is found to be significant for long-range scattering potentials. However, this relative higher-order correction will be reduced as the range of scattering potentials becomes small. The correction depends on various effects, such as the magnetic field, electron and impurity densities, impurity positions, symmetric and asymmetric doping profiles, centre barrier thickness, and degree of interface roughness.

1. Introduction

In a recent letter, one of the authors proposed a mechanism for giant low-temperature magneto-conductance mechanism in a closely tunnel-coupled double-quantum-wire structure [1]. The impurity-limited conductance was shown to be enhanced abruptly by as much as two orders of magnitude within a narrow range of applied magnetic field. The double quantum wires which are stacked in the z-direction and extended along the y-direction are created by adding a lateral confinement to GaAs double quantum wells (QWs) in the x-direction. The lateral confinement is achieved by depositing split metal gates on the front and back of the double QWs (DQWs) of well widths b, which deplete the electrons underneath the gates when a negative voltage is applied. The thickness L_B of the AlGaAs centre barrier between the two QWs is small (e.g., 15–50 Å), allowing electrons to tunnel in the z-direction. In this paper, we consider an extreme quantum size limit where only the ground sublevel from the x-confinement and the ground tunnel-split doublet from the z-confinement are relevant. The magnetic field $\vec{B} = (B, 0, 0)$ is applied in the x-direction. Recently, Vurgaftman and Meyer [2] (VM) studied the conductance enhancement arising from the interface-roughness scattering. By using a two-dimensional finite-difference wave-packet technique and a single-particle approximation, they obtained a much smaller conductance enhancement than predicted by the Born approximation [1] in the presence of interface-roughness scattering. Therefore, it is necessary to examine the effects of higher-order corrections to the Born approximation. We find that corrections to the enhancement can be very large for long-range scattering potentials and can reduce the enhancement by one order of magnitude when the interaction range is of the order of the

0953-8984/00/143383+14$30.00 © 2000 IOP Publishing Ltd

well-to-well separation. However, for short-range impurity potentials, the corrections are much smaller and the conductance enhancement can still be one to two orders of magnitude as predicted by Lyo [1], depending on the impurity positions. For interface-roughness scattering, the enhancement can be much smaller even in the Born approximation when the roughness occurs at least at one of the interfaces of the centre barrier (e.g., GaAs/AlGaAs) because there is a significant overlap of the wave functions of the two wells at these interfaces.

The basic idea of the conductance enhancement in the presence of impurity scattering can be understood from the energy dispersion curves of symmetric double quantum wires at $B = 4.8$ T in figure 1. Here, the dash–dotted curves indicate the energy parabolas of the two QWs in the absence of tunnelling, displaced relative to each other by the magnetic field by $\Delta k = d/\ell^2$ where $d = b + L_B$ is the well-to-well separation and $\ell = (\hbar/eB)^{1/2}$ is the magnetic length. The degeneracy at the crossing point is removed due to tunnelling, opening an anticrossing gap which separates the upper and lower branches shown by the solid curves. The gap moves up in energy as the diamagnetic energy increases with B and crosses the chemical potential μ [1]. The chemical potential is shown by a horizontal dashed line in figure 1. The Born approximation for the momentum dissipation corresponds to the direct back-scattering of electrons between the initial and final Fermi points k_i and k_f shown by the filled circles. In this case, the confinement wave functions at the two Fermi points are separated and localized in the left and right QWs with a very small overlap, yielding a very small scattering rate for short-range impurity interaction. In contrast, when μ is above the gap, we have two pairs of Fermi points such that the wave functions of the pairs have large amplitudes in the left and right QWs, respectively, yielding a large scattering rate. Also, when μ is below the gap at a higher field, back-scattering occurs inside the same QW, as illustrated by the broken arrows

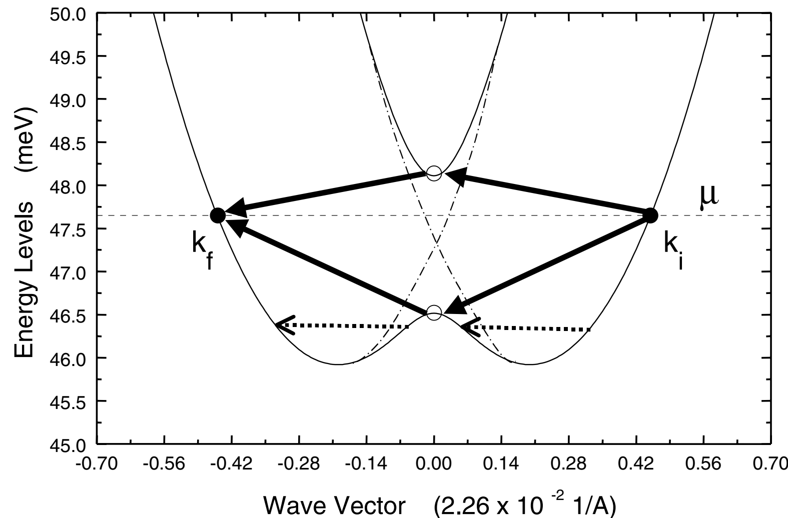

Figure 1. Energy dispersion $E_j^z(k)$ (solid curves) with $j = 1, 2$ at $B = 4.8$ T for $\eta = 0.3$, $b = 80$ Å, $L_B = 50$ Å and a schematic illustration of the two-step impurity back-scattering processes. The dashed horizontal line represents the chemical potential μ at $T = 4$ K for $n_{1D} = 6.5 \times 10^5$ cm^{-1}. The dash–dotted curves are the energy levels in the absence of electron tunnelling between the two wires. The solid arrows indicate the higher-order processes of impurity scattering through the intermediate states (open circles) near the gap edges between the initial (k_i) and final (k_f) states (filled circles) when μ lies inside the gap. The broken arrows represent the impurity back-scattering processes within the quantum wires when μ is below the gap.

in figure 1. Therefore, the scattering rate is relatively large when μ lies outside the gap. As a result, a giant conductance enhancement is obtained in the range of the magnetic field where μ is inside the gap.

The Born approximation may, however, underestimate the scattering rate when μ is inside the gap and overestimate the conductance enhancement. There are higher-order processes which give significant contributions to back-scattering. These processes are illustrated in figure 1 by solid arrows for the case of impurity scattering. In these two-step processes, scattering occurs through the intermediate virtual states near the gap edges (i.e., near $k = 0$) shown by the open circles. These intermediate states have large amplitudes in both QWs, providing a significant simultaneous overlap with the initial- and final-state wave functions at k_i and k_f. For the long-range impurity interaction, the higher-order processes are expected to be more effective because the wave-function overlap between the intermediate states and the initial and final states is no longer limited to a small range around impurity sites. In this paper, we study the effect of the higher-order contributions from impurity and interface-roughness scattering. For both short-range impurity and interface-roughness scattering, the higher-order correction to the enhancement is significant, but the Born approximation is still proved to be qualitatively valid. For long-range scattering potentials, however, the correction is even larger and the Born approximation is no longer valid.

The organization of this paper is as follows. In section 2, we present the formalism for impurity and interface-roughness scattering beyond the Born approximation for the conductance of the electrons in the double quantum wires under a magnetic field. Numerical results and discussion are presented in section 3 for the conductance and enhancement by comparing the results from both the Born approximation and higher-order full theory for impurity and interface-roughness scattering as a function of magnetic field. The paper is concluded in section 4 with some brief remarks.

2. Formalism

Using the Landau gauge for the vector potential $\vec{A} = (0, -Bz, 0)$, the Hamiltonian of the system is given by $\hat{\mathcal{H}} = \hat{\mathcal{H}}_z + \hat{\mathcal{H}}_x$ with

$$\hat{\mathcal{H}}_z = -\frac{\hbar^2}{2}\frac{\partial}{\partial z}\left[\frac{1}{m_e^*(z)}\frac{\partial}{\partial z}\right] + V_{\mathrm{DQW}}(z) + \frac{\hbar^2}{2m_e^*(z)}\left(k - \frac{z}{\ell^2}\right)^2 \tag{1}$$

$$\hat{\mathcal{H}}_x = -\frac{\hbar^2}{2m_W}\frac{\partial^2}{\partial x^2} + V_L(x) \tag{2}$$

where $m_e^*(z)$ is the position-dependent effective mass of electrons in the z-direction, which equals $m_W = 0.0665m_0$ inside the GaAs wells and $m_B = (0.0665 + 0.083\eta)m_0$ inside the $\mathrm{Al}_\eta\mathrm{Ga}_{1-\eta}\mathrm{As}$ barriers with η being the alloy composition index of the ternary barrier material, m_0 is the free electron mass, $V_{\mathrm{DQW}}(z) = 0.57 \times 1.427\eta$ (eV) in the barrier region and zero inside the well, and $V_L(x)$ is the lateral confinement potential of the quantum wires. The last term in equation (1) is the kinetic energy along the wire direction with the wavenumber k. For the Hamiltonian in equations (1) and (2), the electron wave functions can be written as

$$\langle\vec{r}|j,k\rangle = \phi_0(x)\frac{\exp(\mathrm{i}ky)}{\sqrt{L_y}}\psi_{jk}(z) \tag{3}$$

where L_y is the length of the quantum wires. The electrons are assumed to be in the lowest energy eigenstate $\phi_0(x)$ in the x-direction, and the index $j = 1, 2$ stands for the lower and upper tunnel-split branches in the z-direction. The electron energy is given by $\mathcal{E}_{jk} = E_0^x + E_j^z(k)$, where $E_j^z(k)$ is determined by $\hat{\mathcal{H}}_z\psi_{jk}(z) = E_j^z(k)\psi_{jk}(z)$, and E_0^x is the ground level given

by $\hat{\mathcal{H}}_x\phi_0(x) = E_0^x\phi_0(x)$. As seen from the last term in equation (1), the effect of the B-field is to displace the origins of the transverse crystal momenta k in the wire direction in the two quantum wells relative to each other by $\Delta k = d/\ell^2$. The energy dispersion curves $E_j^z(k)$ are displayed in figure 1 for $\eta = 0.3$, $b = 80$ Å, $L_B = 50$ Å, and $B = 4.8$ T.

The conductance is given by

$$G(B) = \frac{2e^2}{L_y^2}\sum_{j,k} v_{jk}\left[-f'(\mathcal{E}_{jk})\right] g_{jk} \tag{4}$$

where $v_{jk} = \hbar^{-1}\,\mathrm{d}E_j^z(k)/\mathrm{d}k$, $g_{jk} = v_{jk}\tau_{jk}$, and τ_{jk} is the relaxation time. The factor of 2 results from the spin summation. In equation (4), $f'(\mathcal{E}_{jk})$ is the first derivative of the Fermi–Dirac distribution function. The quantity g_{jk} represents the linear deviation from the equilibrium Fermi–Dirac distribution and satisfies the Boltzmann equation:

$$v_{jk} - \frac{2\pi}{\hbar}\sum_{m,p}(g_{jk} - g_{mp})\mathcal{I}_{jk,mp}\delta(\mathcal{E}_{jk} - \mathcal{E}_{mp}) = 0 \tag{5}$$

where $\mathcal{I}_{jk,mp} = \mathcal{I}_{jk,mp}^{(0)} + \Delta\mathcal{I}_{jk,mp}$ is the irreducible scattering part shown in figure 2(a) for impurity scattering in the diagrammatic expansion of the current–current correlation function [3] within the ladder approximation. For interface-roughness scattering, an additional two-site diagram shown in figure 2(c) is necessary. The first term $\mathcal{I}_{jk,mp}^{(0)}$, represented by a rung in the left panel of figure 2(a), is the Born approximation while the second term is the higher-order single-site correction described in figure 1. Although this term is of higher order in the scattering potential than the Born term, it occurs without a small direct overlap between the initial and final states in the gap. Instead, the final and initial states are mediated through the intermediate states which have large overlap with both initial and final states as discussed in section 1 and as seen in equation (12). However, we need not consider the third-order contributions shown in figure 2(b) which include a direct overlap between the initial and final states.

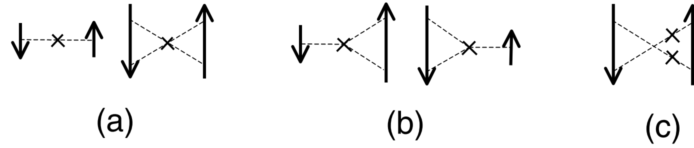

Figure 2. (a) Second-order (left) and fourth-order (right) irreducible impurity scattering parts. (b) These third-order diagrams for impurity scattering are not important for the reason described in the text. (c) The two-site irreducible interface-roughness scattering part.

The conductance expressed in equation (4) yields

$$G(B) = \frac{2e^2}{hL_y}g \tag{6}$$

where g is the sum of g_{jk} over all the Fermi points. An exact solution for g was obtained in reference [1] and is given by replacing $V^2(k, p)$ in equations (5)–(7) of reference [1] with $\mathcal{I}_{jk,mp}$.

For impurity scattering, the Born term in equation (5) is

$$\mathcal{I}_{jk,\ell s}^{(0)} = N_I\int \mathrm{d}^3\vec{R}_\lambda\ \mathcal{P}(\vec{R}_\lambda)\left|u_{jk,\ell s}^\lambda\right|^2 \tag{7}$$

where $\vec{R}_\lambda$ is the position of an individual impurity atom and $\mathcal{P}(\vec{R}_\lambda)$ is the probability density distribution function of the impurity atoms in the system with

$$\int \mathrm{d}^3\vec{R}_\lambda\, \mathcal{P}(\vec{R}_\lambda) = 1.$$

The quantity N_I is the total number of impurities in the system. The matrix element in equation (7) is given by

$$u^\lambda_{jk,mp} = \frac{1}{L_y}\int \mathrm{d}^3\vec{r}\; U^{\mathrm{imp}}(\vec{r}-\vec{R}_\lambda)\phi_0^2(x)\exp[\mathrm{i}(p-k)y]\psi_{jk}(z)\psi_{mp}(z) \tag{8}$$

where $U^{\mathrm{imp}}(\vec{r}-\vec{R}_\lambda)$ is the interaction potential between the electron at $\vec{r}$ and the impurity atom at $\vec{R}_\lambda$. The higher-order scattering part in equation (5) is given by

$$\Delta\mathcal{I}_{jk,\ell s} = N_I\int \mathrm{d}^3\vec{R}_\lambda\, \mathcal{P}(\vec{R}_\lambda)\left|T^\lambda_{jk,\ell s}(\mathcal{E}_{jk})\right|^2 \tag{9}$$

where $T^\lambda_{jk,\ell s}(\mathcal{E})$ includes only the principal part:

$$T^\lambda_{jk,\ell s}(\mathcal{E}) = \sum_{m,p} u^\lambda_{jk,mp}u^\lambda_{mp,\ell s}\frac{(\mathcal{E}-\mathcal{E}_{mp})}{[\mathcal{E}-\mathcal{E}_{mp}]^2+[\Gamma_{mp}(\mathcal{E})]^2}. \tag{10}$$

Here, $\Gamma_{mp}(\mathcal{E})$ is the energy-dependent damping:

$$\Gamma_{jk}(\mathcal{E}) = \pi N_I\sum_{m,p}\int \mathrm{d}^3\vec{R}_\lambda\, \mathcal{P}(\vec{R}_\lambda)\left|u^\lambda_{jk,mp}\right|^2\delta(\mathcal{E}-\mathcal{E}_{mp}). \tag{11}$$

We first assume that the impurities are distributed uniformly on several δ-doping sheets perpendicular to the z-direction [4] with the distribution function given by

$$\mathcal{P}(Z_\lambda) = [C_1\delta(Z_\lambda - z_1) + C_2\delta(Z_\lambda - z_2) + \cdots]/\mathcal{S}$$

where z_i is the impurity sheet position, $\mathcal{S}$ is the area of the impurity sheet, and C_i is the fractional distribution with $C_1 + C_2 + \cdots = 1$. Mostly, we will study a binary distribution (i.e., $C_1 + C_2 = 1$) for various positions of the impurity sheets. Next, we assume that the screened electron–impurity interaction takes a Gaussian form [5]:

$$U^{\mathrm{imp}}(\vec{r}-\vec{R}_\lambda) = U_0\exp\left[-\frac{|\vec{r}-\vec{R}_\lambda|^2}{\Lambda_0^2}\right] \tag{12}$$

where the interaction strength is U_0 and Λ_0 measures the interaction range. Finally, we assume that the lateral confinement of the quantum wires takes a parabolic potential [6] $V_L(x) = m_W\Omega_x^2x^2/2$, yielding

$$\phi_0(x) = \left(\frac{\alpha}{\sqrt{\pi}}\right)^{1/2}\exp\left(-\frac{1}{2}\alpha^2x^2\right) \tag{13}$$

with $\alpha = \sqrt{m_W\Omega_x/\hbar}$. Here $2/\alpha$ represents the confinement width of wave functions in quantum wires. The interaction matrices in equations (7) and (9) are then explicitly given by

$$\mathcal{I}^{(0)}_{jk,\ell s} = \frac{n_I\pi\alpha\Lambda_0^4U_0^2}{L_y\sqrt{1+\alpha^2\Lambda_0^2}}\sqrt{\frac{\pi}{2}}\exp\left[-\frac{1}{2}(s-k)^2\Lambda_0^2\right]\sum_\beta C_\beta\left[W^\beta_{jk,\ell s}\right]^2 \tag{14}$$

$$\Delta\mathcal{I}_{jk,\ell s} = \frac{n_I\pi^2\alpha^3\Lambda_0^8U_0^4}{L_y^3(1+\alpha^2\Lambda_0^2)^{3/2}}\frac{\sqrt{\pi}}{2}\sum_\beta C_\beta\left\{\sum_{m,p}\exp\left(-\frac{1}{4}[(p-k)^2+(s-p)^2]\Lambda_0^2\right)\right.$$
$$\left.\times\frac{(\mathcal{E}-\mathcal{E}_{mp})}{[\mathcal{E}-\mathcal{E}_{mp}]^2+[\Gamma_{mp}(\mathcal{E})]^2}W^\beta_{jk,mp}W^\beta_{mp,\ell s}\right\}^2 \tag{15}$$

where $n_I = N_I/\mathcal{S}$ is the two-dimensional impurity density of the system, and the impurity interaction integral is given by

$$W^{\beta}_{jk,mp} = \int \mathrm{d}z\ \psi_{jk}(z)\psi_{mp}(z)\exp\left[-\frac{1}{\Lambda_0^2}(z-z_\beta)^2\right]. \tag{16}$$

For interface-roughness scattering, its scattering potential takes the following form:

$$V^{\mathrm{IR}}(\vec{r}) = \pm V_0 \sum_{\lambda=1,2} \delta(z - Z_\lambda)\,\delta b_\lambda(\vec{r}_\parallel) \tag{17}$$

where $\lambda = 1, 2$ stands for the two rough interfaces from the AlGaAs to the GaAs layer in DQWs during the MBE growth, Z_λ is the position of the rough interfaces, V_0 is the well depth, $\delta b_\lambda(\vec{r}_\parallel)$ is the layer fluctuation, and $\vec{r}_\parallel$ is the position vector within the interfaces. The potential in equation (17) yields the well-known expression $(\partial E/\partial b_\lambda)\,\delta b_\lambda$ for arbitrary V_0 [7]. By assigning a Gaussian form to the n-site correlation function of layer fluctuations:

$$\langle \delta b_\lambda(\vec{r}_{1\parallel})\,\delta b_\lambda(\vec{r}_{2\parallel})\cdots\delta b_\lambda(\vec{r}_{n\parallel})\rangle = (\delta b_\lambda)^n \sqrt{\frac{n}{\pi\mathcal{L}^2}} \int \mathrm{d}^2\vec{r}_\parallel \prod_{i=1}^{n} \exp\left[-\frac{(\vec{r}_\parallel - \vec{r}_{i\parallel})^2}{\mathcal{L}^2}\right] \tag{18}$$

we find

$$\mathcal{I}^{(0)}_{jk,\ell s} = \frac{\sqrt{\pi}\alpha\,\delta b^2\,\xi^2 V_0^2}{L_y\sqrt{2+\alpha^2\xi^2}} \exp\left[-\frac{1}{4}(s-k)^2\xi^2\right] \sum_{\lambda=1,2} \left[\psi_{jk}(Z_\lambda)\psi_{\ell s}(Z_\lambda)\right]^2 \tag{19}$$

$$\begin{aligned}
\Delta\mathcal{I}_{jk,\ell s} = {} & \frac{\pi^{3/2}\alpha^3\,\delta b^4\,\xi^6 V_0^4}{\sqrt{2}L_y^3(2+\alpha^2\xi^2)^{3/2}} \sum_{\lambda=1,2} \left[\psi_{jk}(Z_\lambda)\psi_{\ell s}(Z_\lambda)\right]^2 \\
& \times \left\{ \sum_{m,p} \exp\left(-\frac{1}{8}[(p-k)^2 + (s-p)^2]\xi^2\right) \right. \\
& \left. \times \frac{(\mathcal{E}-\mathcal{E}_{mp})}{[\mathcal{E}-\mathcal{E}_{mp}]^2 + [\Gamma_{mp}(\mathcal{E})]^2} \left[\psi_{mp}(Z_\lambda)\right]^2 \right\}^2 \\
& + \frac{\pi\alpha^2\,\delta b^4\,\xi^4 V_0^4}{L_y^2(2+\alpha^2\xi^2)} \sum_{m,p;m',p'} \delta_{p+p',k+s} \exp\left[-\frac{1}{4}(k-p)^2\xi^2\right] \exp\left[-\frac{1}{4}(k-p')^2\xi^2\right] \\
& \times \frac{(\mathcal{E}-\mathcal{E}_{mp})}{[\mathcal{E}-\mathcal{E}_{mp}]^2 + [\Gamma_{mp}(\mathcal{E})]^2} \frac{(\mathcal{E}-\mathcal{E}_{m'p'})}{[\mathcal{E}-\mathcal{E}_{m'p'}]^2 + [\Gamma_{m'p'}(\mathcal{E})]^2} \\
& \times \left\{ \sum_{\lambda=1,2} \left[\psi_{jk}(Z_\lambda)\psi_{\ell s}(Z_\lambda)\right] \left[\psi_{mp}(Z_\lambda)\psi_{m'p'}(Z_\lambda)\right] \right\}^2
\end{aligned} \tag{20}$$

where $\xi = \sqrt{2}\mathcal{L}$ is the correlation length of the interface roughness,

$$\Gamma_{jk}(\mathcal{E}) = \pi \sum_{m,p} \mathcal{I}^{(0)}_{jk,mp}\delta(\mathcal{E}-\mathcal{E}_{mp}) \tag{21}$$

and δb is the average displacement of the rough interface. Note that the right-hand side of equation (18) yields $(\delta b_\lambda)^n$ for $\vec{r}_{1\parallel} = \vec{r}_{2\parallel} = \cdots = \vec{r}_{n\parallel}$. Equation (18) reduces to the standard expression $\exp[-(\vec{r}_{1\parallel} - \vec{r}_{2\parallel})^2/\xi^2]$ for $n = 2$. In equation (20), the first term corresponds to the single-site correction given by the right-hand panel of figure 2(a) and the second term to the two-site correction given by figure 2(c). It is clear from equations (19) and (20) that the factor of small direct overlap $[\psi_{jk}(Z_\lambda)\psi_{\ell s}(Z_\lambda)]^2$ at the two rough layers between the initial and final states in the anticrossing gap is equally kept in $\mathcal{I}^{(0)}_{jk,\ell s}$ and $\Delta\mathcal{I}_{jk,\ell s}$ due to the contacting potential in equation (17).

3. Numerical results and discussion

In this section, we present numerical results for the B-dependent conductance and its enhancement. Several different structures of double quantum wires as well as doping and roughness configurations are considered to bring out salient features of the results.

In the following numerical calculations, we consider three samples. Sample 1 is the doped symmetric AlGaAs/GaAs DQW with impurity density $n_I = 8.12 \times 10^8$ cm^{-2}, well depth $V_0 = 280$ meV, well width $b = 80$ Å, and wire confinement width $2/\alpha = 42$ Å. The effective mass of electrons is $m_W = 0.067m_0$ ($m_B = 0.073m_0$) in the wells (barriers). The centre barrier thickness is $L_B = 50$ Å, and the tunnelling gap Δ_{SAS} at $B = 0$ is 1.6 meV. The impurity interaction strength is $U_0 = 1.26$ eV. Sample 2 has the same parameters as those of sample 1 except that the centre barrier thickness is $L_B = 40$ Å and the tunnelling gap at $B = 0$ is 3.6 meV. Sample 3 is a modulation-doped DQW with interface roughness. It has $V_0 = 250$ meV and $L_B = 40$ Å. The parameters of sample 3 are the same as those in reference [2]. $\Delta_{SAS} = 3.6$ meV at $B = 0$. The correlation length is $\xi = 30$ Å, and the average displacement $\delta b = 5$ Å. However, the one-dimensional electron density here is $n_{1D} = 6.5 \times 10^5$ cm^{-1} which is smaller than that in reference [2]. The quantities m_B, m_W, b, and $2/\alpha$ for sample 3 are the same as those for sample 1. The calculations are performed at $T = 4$ K. Other parameters used in the calculation will be given in the corresponding figure captions.

The quantities $G(B)$ in arbitrary units are compared for doped samples 1 and 2 with impurity scattering in figure 3. Here, $n_{1D} = 6.5 \times 10^5$ cm^{-1} and $\Lambda_0 = 12$ Å. A giant enhancement of the conductance is obtained when μ lies inside the anticrossing gap in the range of the fields between 4.2 T and 6.0 T for sample 1 and 3.2 T and 7.4 T for sample 2.

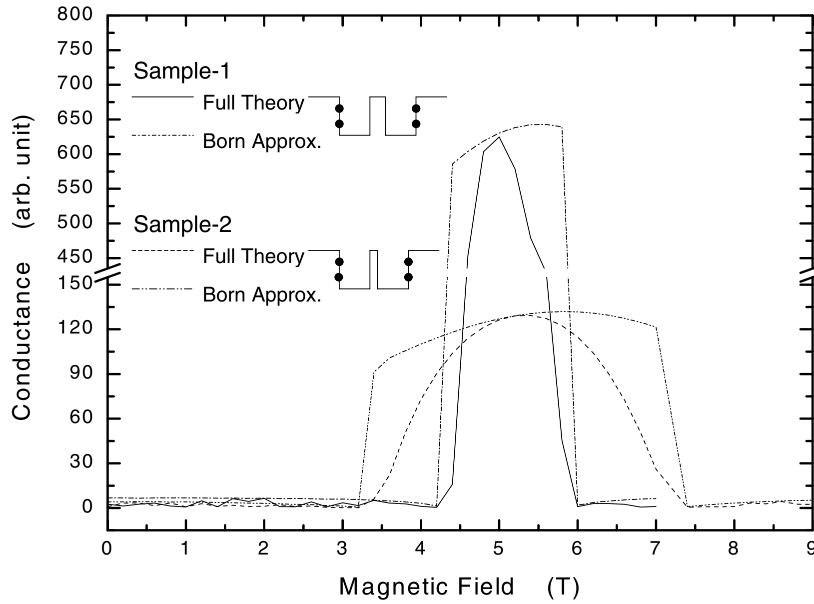

Figure 3. $G(B)$ (solid and dashed curves) and $G^{\mathrm{Born}}(B)$ (dash–dotted and dash–dot–dotted curves) in arbitrary units for doped samples 1 and 2 as functions of B for $n_{1D} = 6.5 \times 10^5$ cm^{-1}, $\Lambda_0 = 12$ Å, and $n_I = 8.12 \times 10^8$ cm^{-2}. In the figure, the two impurity sheets sit at the outer interfaces of the DQWs with $C_1 = C_2 = 0.5$.

The wave functions of sample 2 at the two Fermi points inside the gap have much larger overlap with the impurities, leading to the reduction of $G(B)$ inside the gap compared to that of sample 1. For sample 1, the effect of higher-order correction to the conductance peak is visible. Increased electron tunnelling reduces this correction for sample 2. This reduction is caused by the enhanced damping arising from larger wave-function overlap at the impurity sites. Around the middle of the gap, the higher-order correction reaches a minimum. This is due to the cancellation between the positive and negative contributions to the numerator $\mathcal{E}-\mathcal{E}_{mp}$ in equation (10) from the intermediate states near both edges of the gap. Therefore, the higher-order correction is suppressed there. However, the energy difference $\mathcal{E}-\mathcal{E}_{mp}$ in equation (10) between the initial/final state and the intermediate states around the edges of the gap becomes comparable to or smaller than the damping $\Gamma_{mp}(\mathcal{E})$. This enhances the higher-order correction and reduces the conductance around the edges of the gap. Small fluctuations of the curves in figure 3 are due to the numerical fluctuations arising from using a finite number of k-points in the numerical evaluation. By including the damping effect in the Boltzmann equation in equation (5), the shape of the curves around the edges of the gap will be slightly modified due to the enhancement of the damping contribution there. However, the peak conductance around the middle of the gap remains unchanged.

While $G(B)/G(0)$ is independent of n_I for impurity scattering in the Born approximation, the higher-order contributions depend on n_I through the energy-dependent damping in equation (11). The effect of the higher-order correction is smaller outside the gap for larger n_I. This is due to the fact that back-scattering through the intermediate states becomes suppressed when the damping $\Gamma_{mp}(\mathcal{E}_{jk}) \propto n_I$ in the denominator of equation (10) becomes large. When the two impurity sheets are moved slightly from the outer interfaces of the QWs into the outer barriers, $G(B)$ is increased significantly inside the gap although there is almost no change outside the gap. In this case, the impurity interaction in equation (16) is reduced when μ is inside the gap. This explains the increase of $G(B)$. If the impurities are distributed from the two outer interfaces to all over the four interfaces of the DQWs while keeping the total number of impurities the same, $G(B)$ with two impurity sheets will be large inside the gap compared with that with four impurity sheets. This is due to the enhanced impurity interaction in equation (16) at the centre barrier when μ is inside the gap.

$G(B)/G(0)$ is compared in figure 4 for symmetric and asymmetric impurity doping in sample 1. Here, $n_{1D} = 6.5 \times 10^5$ cm^{-1} and $\Lambda_0 = 12$ Å. On changing from symmetric to asymmetric doping, $G(B)/G(0)$ remains the same inside the gap but increases slightly outside the gap (see the lower-left inset). The increased $G(B)/G(0)$ outside the gap for asymmetric doping can be explained in the following way [1, 8]. Under a large B, the wave functions at the Fermi points become separated into either one of the QWs resembling two parallel resistors with individual resistance R_0 and combined resistance $R_0/2$ for symmetric doping. For asymmetric doping, the resistance of the two channels becomes $R_0 \pm \Delta R$, yielding a total resistance $(R_0^2 - \Delta R^2)/2R_0 < R_0/2$. This implies that the asymmetric doping with $\Delta R \neq 0$ has the smaller total resistance or the larger total conductance compared to that of the symmetric doping. That is, more current flows through the channel with fewer impurities and a higher conductance, increasing the total conductance. However, at $B = 0$ or inside the gap, the conductance depends only on $C_1 + C_2$ (which equals 1), yielding the same enhancement inside the gap for symmetric and asymmetric doping. If the higher-order correction is included, we find that the conductance enhancement around the middle of the gap is increased compared to that of the Born approximation mainly because $G(0) < G^{\mathrm{Born}}(0)$ while $G(B) \approx G^{\mathrm{Born}}(B)$ inside the gap.

We show in figure 5 the dependence of $G(B)$ in arbitrary units on the electron density n_{1D} for doped sample 1 with $\Lambda_0 = 12$ Å. When n_{1D} is decreased from 6.5×10^5 cm^{-1}

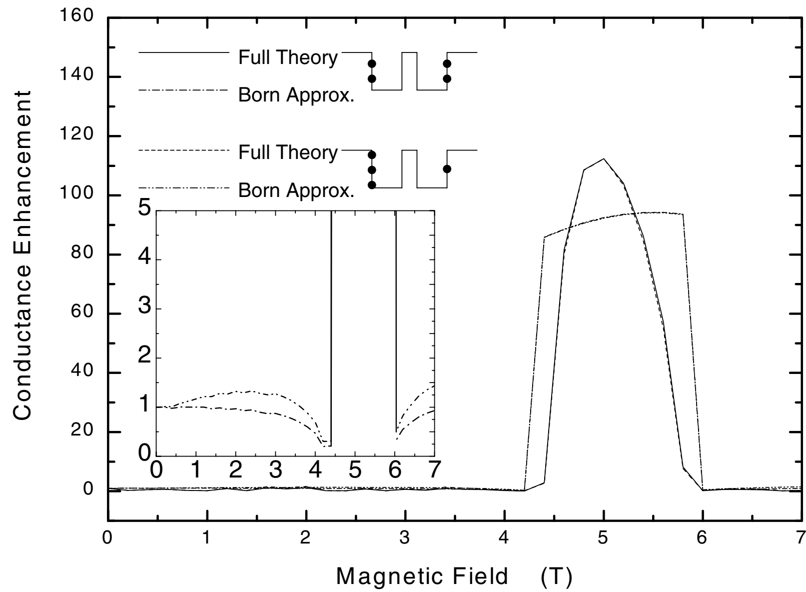

Figure 4. $G(B)/G(0)$ (solid and dashed curves) and $G^{\mathrm{Born}}(B)/G^{\mathrm{Born}}(0)$ (dash–dotted and dash–dot–dotted curves) for doped sample 1 as functions of B with symmetric and asymmetric impurity distributions. For symmetric and asymmetric doping, we set $C_1 = C_2 = 0.5$ and $C_1 = 0.75$, $C_2 = 0.25$, respectively. The two impurity sheets are put at the outer interfaces of the DQWs. The inset displays on an amplified scale $G^{\mathrm{Born}}(B)/G^{\mathrm{Born}}(0)$ outside the gap for symmetric and asymmetric doping. The values of n_{1D}, Λ_0, and n_I are the same as those for figure 3.

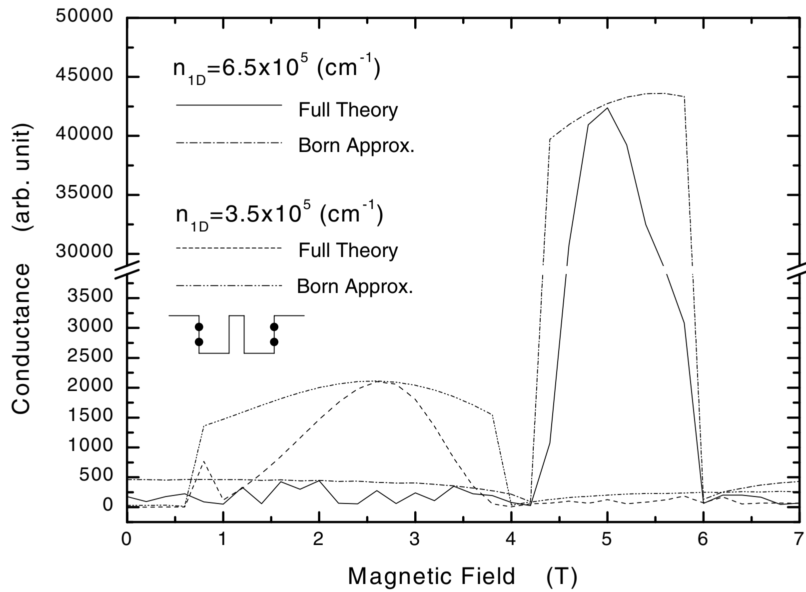

Figure 5. $G(B)$ (solid and dashed curves) and $G^{\mathrm{Born}}(B)$ (dash–dotted and dash–dot–dotted curves) in arbitrary units for doped sample 1 as functions of B with different electron densities. For high- and low-density samples, we set $n_{1D} = 6.5 \times 10^5$ cm^{-1} and $n_{1D} = 3.5 \times 10^5$ cm^{-1}, respectively. The two impurity sheets are at the outer interfaces of the DQWs with $C_1 = C_2 = 0.5$. The values of Λ_0 and n_I are the same as those for figure 3.

to 3.5×10^5 cm^{-1}, the onset of the gap-enhancement region is shifted from $B = 4.2$ T to $B = 0.6$ T due to the reduction of μ. The great reduction of $G(B)$ inside the gap for the low-density sample is a result of the large overlap between the wave functions at the two Fermi points due to the fact that the separation of the wave functions into the two QWs is far from complete at low B-fields. Although the conductance enhancement at the middle of the gap is increased for the high-density sample compared to that of the Born approximation because $G(0) < G^{\rm Born}(0)$, this difference between the Born approximation and the full theory is decreased for the low-density sample. This is because of the relatively large damping at the middle of the gap due to the incomplete separation of the wave functions into the two QWs at low B-fields.

In figure 6, we show $G(B)/G(0)$ for doped sample 1 with different positions of the impurity sheets in the centre barrier. Here, $n_{1D} = 6.5 \times 10^5$ cm^{-1} and $\Lambda_0 = 12$ Å. When the two impurity sheets are moved inwards symmetrically by 5 Å from the interfaces of the middle barrier, $G(B)/G(0)$ decreases significantly inside the gap but changes by only a small amount outside the gap. Because the wave function of the upper branch is independent of k and antisymmetric at $B = 0$, it has only a small amplitude at the impurity sites near the centre of the middle barrier. As a result, $G(0)$ is greatly increased when the two impurity sheets are pushed towards the centre of the middle barrier. On the other hand, this antisymmetry is absent at high B-fields when μ lies within the gap. Consequently, $G(B)/G(0)$ is reduced inside the gap mainly due to the large value of $G(0)$. As the range of the impurity potential is increased, this effect is expected to be weakened because the wave-function overlap can go far beyond the impurity sites. When the higher-order correction is included, we find that the conductance enhancement around the middle of the gap is increased compared to that of the Born approximation because $G(0) < G^{\rm Born}(0)$ and $G(B) \approx G^{\rm Born}(B)$ inside the gap at the same time.

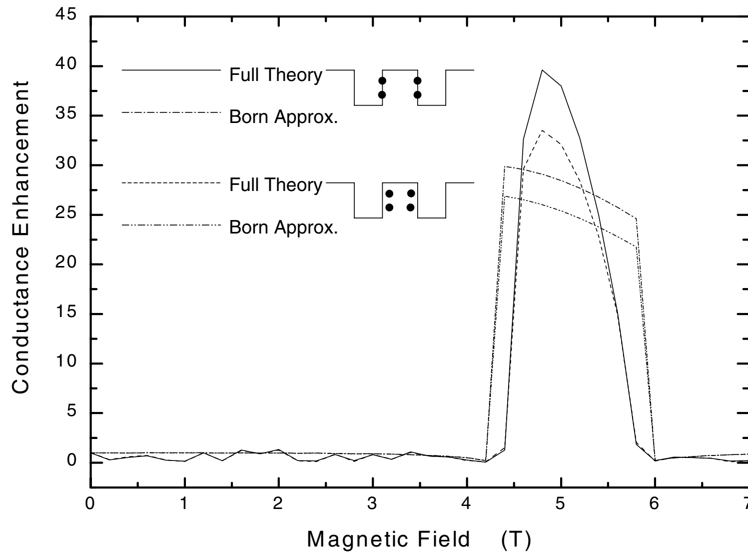

Figure 6. $G(B)/G(0)$ (solid and dashed curves) and $G^{\rm Born}(B)/G^{\rm Born}(0)$ (dash–dotted and dash–dot–dotted curves) for doped sample 1 as functions of B with two positions of the impurity sheets at the centre barrier: one sample with impurity sheets at the two interfaces of the middle barrier and the other sample with impurity sheets at 5 Å away from the interfaces inside the middle barrier. The values of n_{1D}, Λ_0, and n_I are the same as those for figure 3.

As discussed earlier with reference to figure 1, the higher-order corrections are expected to be more significant for long-range scattering potentials. In order to demonstrate this effect, we compare $G(B)/G(0)$ with $G^{\mathrm{Born}}(B)/G^{\mathrm{Born}}(0)$ for sample 1 in figure 7 with $n_{1D} = 6.5 \times 10^5$ cm^{-1} for different ranges of the scattering potential. When $\Lambda_0 = 80$ Å, the enhancement inside the gap is reduced significantly. The effect is more pronounced for $\Lambda_0 = 120$ Å. Another effect which influences the result is that the long-range interaction disfavours the large momentum transfer. This effect is clearly seen in figure 7 where the enhancement for $\Lambda_0 = 120$ Å (dash–dot–dotted curve) is much larger than that for $\Lambda_0 = 80$ Å (dash–dotted curve) inside the gap in the Born approximation. This is due to the fact that the momentum transfer for $2k_f$-back-scattering in the Born approximation is very large in the gap (compared to that at $B = 0$), reducing the scattering rate much more for $\Lambda_0 = 120$ Å than for $\Lambda_0 = 80$ Å. The curves for the full theory in figure 7 are, however, dominated by the higher-order corrections which rely on the momentum transfer of $\sim k_f$ which is about the same as the momentum transfer at $B = 0$, yielding similar enhancements for both $\Lambda_0 = 120$ Å and $\Lambda_0 = 80$ Å.

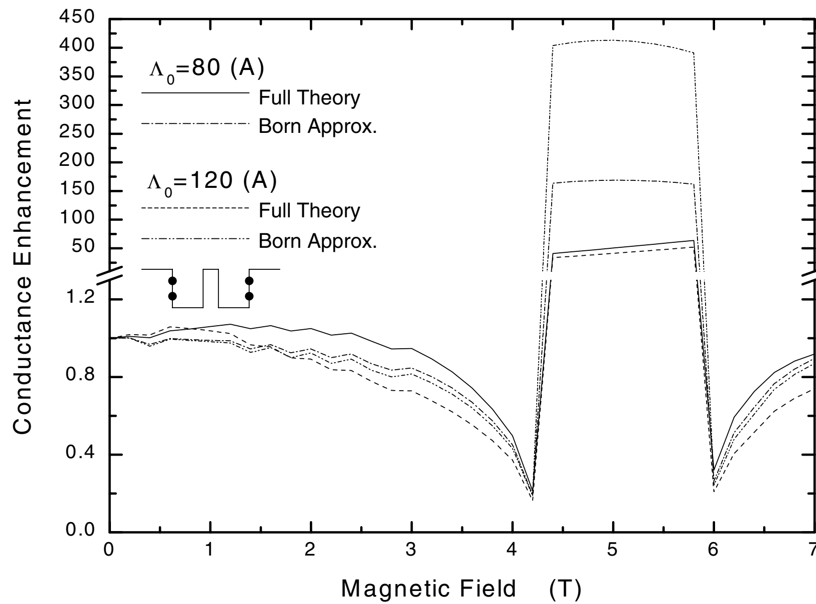

Figure 7. $G(B)/G(0)$ (solid and dashed curves) and $G^{\mathrm{Born}}(B)/G^{\mathrm{Born}}(0)$ (dash–dotted and dash–dot–dotted curves) for doped sample 1 as functions of B with different impurity interaction ranges: one sample with $\Lambda_0 = 80$ Å and the other one with $\Lambda_0 = 120$ Å; two impurity sheets at the outer interfaces of the DQWs with $C_1 = C_2 = 0.5$. The values of n_{1D}, Λ_0, and n_I are the same as those for figure 3.

In the following we restrict our study to the interface-roughness scattering in modulation-doped sample 3 in order to compare our result with the simulation result of VM [2]. Figure 8 displays $G(B)$ in arbitrary units, including the higher-order corrections for samples with different positions of the rough interfaces. The sample with one of the rough interfaces at the middle barrier corresponds to that studied by VM. For this sample, we note remarkable differences between our results and those obtained by VM. First, the enhancement inside the gap from the Born approximation in figure 8 is about 13 which is more than one order of magnitude smaller than that obtained by VM. This may be due to the fact that VM's sample

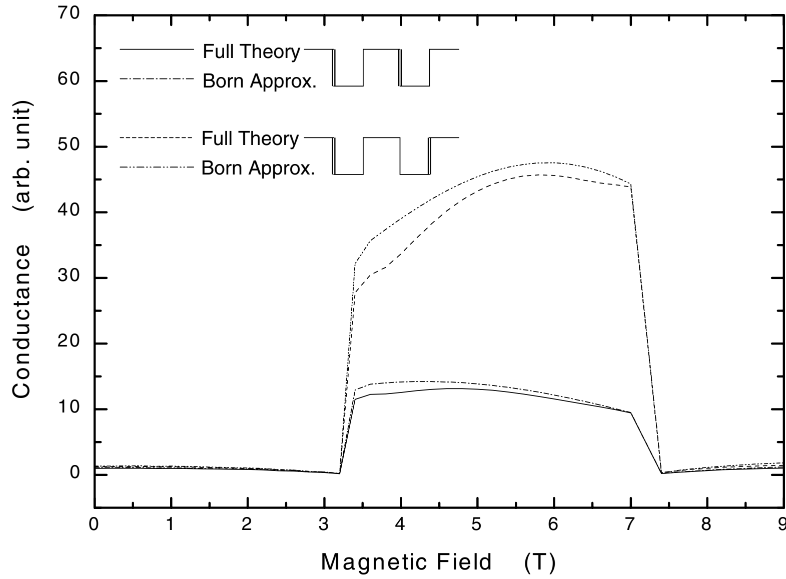

Figure 8. $G(B)$ (solid and dashed curves) and $G^{\mathrm{Born}}(B)$ (dash–dotted and dash–dot–dotted curves) in arbitrary units for modulation-doped sample 3 as functions of B with two positions of rough interfaces. The rough interfaces are illustrated by the doubled line. The parameters used are: $L_B = 40$ Å, $b = 80$ Å, $2/\alpha = 42$ Å, $\xi = 30$ Å, $\delta b = 5$ Å, $V_0 = 250$ meV, and $n_{1D} = 6.5 \times 10^5$ cm^{-1}; one sample with one of the rough interfaces at the middle barrier and another sample with both rough interfaces at the outer barriers.

has much higher n_{1D}, so μ enters the gap at very high B-fields, making the wave functions more completely separated. Second, the Born approximation is reasonably accurate at all B-fields in contrast to VM's result. For the sample with both rough interfaces at the outer barriers, however, the higher-order corrections reduce the conductance somewhat more inside the gap (e.g., by about 10%). The main higher-order contribution arises from the second term in equation (15). The enhancement for this case is very large mainly because the roughness is at the outer barrier interfaces. Our n_{1D} in figure 8 is smaller than that used by VM [2]. For larger n_{1D}, a larger number of k-points is necessary for the same accuracy, increasing the computing time beyond our capability.

For impurity scattering, the damping effect can be made negligible if we keep the impurity density n_I low enough. For interface-roughness scattering, the enhancement is smaller compared to the case of scattering from remote impurities, because the scattering centres are close to the QWs. The damping Γ is another factor that restricts the maximum attainable enhancement for interface-roughness scattering. The idea of enhancement is based on a well-defined anticrossing gap $\Delta_{\mathrm{SAS}} \gg \Gamma$. This condition is not satisfied for samples with a wide centre barrier, although a very large enhancement may be obtained in this case. The smallness of the ratio $r = \Gamma/\Delta_{\mathrm{SAS}} \ll 1$ is also assumed in equation (5). While Γ can be made very small for impurity scattering in principle by modulation doping, some degree of Γ from interface-roughness scattering is unavoidable at present due to growth problems. Damping modifies the δ-function into a Lorentzian function, allowing non-energy-conserving scattering via the Lorentzian wings in equation (5). This higher-order scattering ($\sim r$) may not be negligible when the Fermi points lie near the middle of the gap. In this case, the direct overlap $\sim 1/f_\delta$ between the initial and final wave functions is small for resonant scattering between the two Fermi points as

discussed already. Here, f_δ is the large Born enhancement factor with the δ-function in equation (5). In the non-energy-conserving processes, the electron is scattered from the initial Fermi point near the centre of the gap to the gap edge of the upper branch, thus avoiding the small wave-function overlap of the resonant scattering introduced by the δ-function approximation. A quantitative calculation of this effect is beyond our present numerical capability. Therefore, we carry out an order-of-magnitude estimation by comparing the two contributions in the scattering part. The effect of these non-energy-conserving processes is to modify the effective enhancement f roughly by $1/f = 1/f_\delta + (r/4\pi s)$. Here, $s = 1$ ($s = 4$) for the short-range (long-range) scattering potential. The damping correction can be neglected in the limit of $f_\delta(r/4\pi s) \ll 1$. In the opposite limit, the enhancement becomes $\sim(4\pi s/r)$ which is still large when $r \ll 1$. For the two samples with interface roughness and $\Delta_{SAS} = 3.67$ meV in figure 8, we find $f_\delta(r/4\pi) = 0.15 \ll 1$ for the sample with a smaller enhancement $f_\delta = 14$ and $f_\delta(r/4\pi) = 0.49 < 1$ for the sample with a larger enhancement $f_\delta = 36$. The ratio $f_\delta(r/4\pi)$ can be even smaller for samples with smoother interfaces, making the Born δ-function approximation more accurate. The criterion $f_\delta(r/4\pi s) \ll 1$ has been well satisfied in figures 3–7.

4. Conclusions and remarks

For impurity scattering, the effect of higher-order corrections to the Born approximation was studied for the giant conductance enhancement in tunnel-coupled double quantum wires in a magnetic field. The relative correction to the enhancement at the middle of the gap was found to be significant for the short-range impurity potential, and become even larger for the long-range impurity potential. The effects of weak localization and Coulomb interaction on the electron energy levels have been neglected. Various effects have been found to play a role in the conductance enhancement. These effects include the impurity and electron densities, level damping, positions of the impurity sheets, symmetric and asymmetric impurity distribution, and the centre barrier thickness. The higher-order corrections consist of processes of two-step back-scattering through the virtual intermediate states near the gap edges. These processes increase the overlap of the wave functions at the two Fermi points inside the gap with the impurities and reduce the conductance enhancement compared to that of the Born approximation.

The effect of interface-roughness scattering on the conductance enhancement was also studied beyond the Born approximation. In this case, the Born approximation is found to be still valid as long as the level damping is much smaller than the anticrossing gap. The relative correction to the enhancement inside the gap was found to reach as much as 10%. Several effects, such as correlation length, average displacement of interface, centre barrier thickness, and position of the rough interfaces, have been found to affect the conductance enhancement. The enhancement in the gap is very large for samples with both rough interfaces at the outer barriers as shown in figure 8. However, for samples with one of the rough interfaces at the edges of the centre barrier (e.g., GaAs/AlGaAs QWs), the enhancement is much smaller, but is still larger than that found by VM [2]. In their paper, only the numerical result was shown, and the physics behind the result is unclear.

Acknowledgments

Sandia is a multiprogramme laboratory operated by Sandia Corporation, a Lockheed-Martin Company, for the US DOE under Contract No DE-AC04-94AL85000.

References

[1] Lyo S K 1996 *J. Phys: Condens. Matter* **8** L703
The quantity $u_{1-,2+}$ in the first parentheses on the right-hand side of equation (6) should read: $u_{1-,2-}$.
[2] Vurgaftman I and Meyer J R 1997 *J. Appl. Phys.* **82** 3881
[3] Mahan G D 1981 *Many-Particle Physics* (New York: Plenum) ch 7.1, pp 591–622
[4] Esfarjani K and Glyde H R 1990 *Phys. Rev.* B **41** 1042
[5] Ando T, Fowler A B and Stern F 1982 *Rev. Mod. Phys.* **54** 437
[6] Plaut A S, Lage H, Grambow P, Heitmann D, von Klitzing K and Ploog K 1991 *Phys. Rev. Lett.* **67** 1642
[7] Sakaki H, Noda T, Hirakawa K, Tanaka M and Matsusue T 1987 *Appl. Phys. Lett.* **51** 1934
Lyo S K 2000 to be published
[8] Palevski A, Beltram F, Capasso F, Pfeiffer L N and West K W 1990 *Phys. Rev. Lett.* **65** 1926